Propagation and density effects in the coherent-population-trapping maser

Aldo Godone,[1] Filippo Levi,[1] and Salvatore Micalizio[2]
[1]*Istituto Elettrotecnico Nazionale Galileo Ferraris, Torino, Italy*
[2]*Politecnico di Torino, Torino, Italy*
(Received 7 August 2001; published 4 February 2002)

The coherent microwave emission from an optically thick atomic ensemble in a cavity under coherent population trapping is analyzed. Transient and continuous operations are theoretically examined within the frame of a closed three-level system in the Dicke regime. The effects related to the atomic density and to the propagation in the active medium are examined with particular reference to the subnatural linewidth, the low group velocity and the shifts of the maser emission profile from the unperturbed atomic transition. The case of alkali-metal atoms submitted to a Λ excitation scheme is addressed in view of applications in the atomic frequency standard field. Experimental observations in agreement with the theoretical predictions are reported for the case of rubidium in a buffer gas. Apparent superluminal propagation is also reported and briefly discussed.

DOI: 10.1103/PhysRevA.65.033802 PACS number(s): 42.50.Gy, 32.70.Jz, 42.62.Fi, 06.30.Ft

I. INTRODUCTION

The phenomenon of coherent population trapping (CPT) in an atomic medium has been widely examined in the literature since the observation of dark lines in the fluorescence spectrum of Na atoms submitted to a Λ excitation scheme [1]. The coupling of the two hyperfine ground-state levels of an alkali atom to an excited state via two resonant laser radiations drives the atomic ensemble into a nonabsorbing state: the light transmission of the medium is no longer described by the classical Beer's law and the electromagnetically induced transparency (EIT) effect mainly characterizes the atomic ensemble [2,3]. Moreover, the atoms are coherently trapped in the ground-state sublevels and the strong coherence induced between them is responsible of the coherent microwave emission observed when this atomic ensemble (phaseonium [2]) is coupled to a cavity tuned to the hyperfine frequency [4].

This system behaves as a passive maser (CPT maser) and, besides its physical interest, may find application in the atomic frequency standard field as a microwave oscillator with high medium-term stability [5]. A theoretical analysis of the CPT maser has been reported in the long-wavelength approximation [6] for the case of negligible feedback of the cavity on the atomic medium assumed optically thin. Under these hypothesis no population unbalance is present between the ground-state levels and the coherent emission takes place without population inversion. This highly symmetric condition strongly reduces the cavity pulling and the light shift effects that are responsible at a good extent of the medium-term frequency instability of the intensity pumped maser and of the optical-rf double-resonance passive standards.

A strong field self-consistent approach has been developed in [7] where the feedback of the cavity on the atomic ensemble is fully taken into account; it introduces radiation damping and an unbalance in the populations of the ground state decreasing the intrinsic symmetry of the excitation Λ scheme.

In order to fully describe the behavior of a CPT maser it is necessary to remove the long-wavelength approximation and the hypothesis of optically thin medium; in fact, relevant density and propagation effects have been observed for the case of dark transitions even at temperatures lower than 60 °C for Rb and 40 °C for Cs, as reported, for example, in [8].

In this paper we extend the self-consistent theoretical approach of the CPT maser to the case of an optically thick active medium whose spatial dimensions are comparable to the microwave wavelength. The theory will be developed for a closed three-level system in presence of a buffer gas mixture containing N_2 to reduce the emission profile linewidth by Dicke narrowing and to avoid radiation trapping effects [9] by quenching the fluorescence light scattered by the atomic ensemble. In particular, the following points have to be taken into account: (i) the traveling wave laser beams used for the Λ excitation scheme have a relative phase that changes in a significant way along the propagation axis, inside the active medium; (ii) the phase of the microwave radiation emitted by each atom is referred to the local optical phase difference; (iii) due to the fact that the microwave field inside the cavity is a standing wave, each atom is coupled to the microwave field generated by the whole atomic ensemble.

In this paper, the influence of the atomic density and of the length of the active medium on the emitted power and on the emission profile will be made clear; among others, a new frequency shift is found related to the propagation of the laser beams inside the active medium and the possibility of reaching subnatural linewidth is predicted in the case of a pure three-level system. Nevertheless, in view of possible metrological applications of the CPT maser, it appears possible to reduce the effects induced by the cavity feedback on the maser emission profile through a proper choice of the operating parameters.

A comparison is made also with the intensity optically pumped (IOP) alkali-atom maser, which allows a better understanding of the CPT maser behavior.

Finally we report the experimental results that confirm the theoretical predictions both in transient and in continuous operation in the case of ^{87}Rb in buffer gas and, in particular, the observation of the propagation shift, of the subnatural

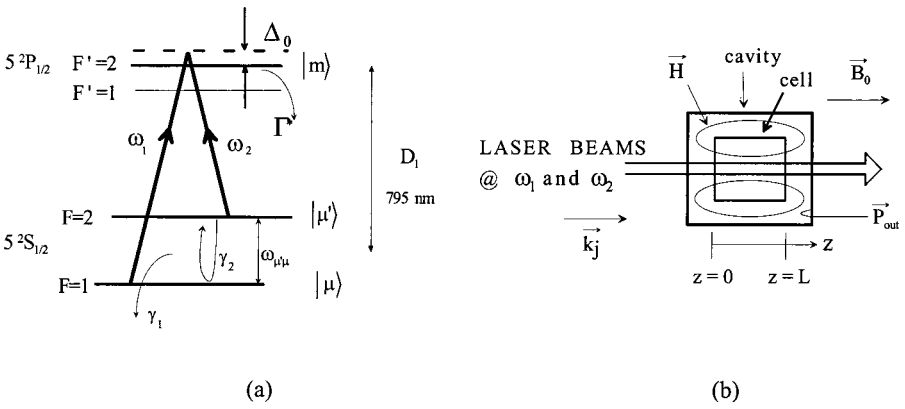

FIG. 1. Energy levels (a) and schematic illustration of the setup (b) considered in the theoretical analysis.

linewidth and of very low and even negative group velocities.

II. THEORY

The analysis is performed for the energy-level scheme shown in Fig. 1(a); the diagram is typical of alkali-metal atoms and the figure addresses the particular case of ^{87}Rb D_1 optical transition, even if the theory may be easily extended to any closed three-level system. In the analysis we consider the setup illustrated in Fig. 1(b) where the atomic ensemble submitted to a Λ excitation scheme is coupled to a microwave cavity tuned to the hyperfine frequency.

We consider two copropagating laser beams with wave vectors $\vec{k}_j = k_j \hat{z}$ $(j=1,2)$ and with a common polarization $\hat{e}_\lambda$ independent of z; we assume also for the field amplitudes spatial variations only along the z axis, so that we can write,

$$\vec{E}_j = E_j(z,t)\hat{e}_\lambda; \quad \hat{e}_\lambda \cdot \hat{z} = 0; \quad \vec{\nabla}\cdot\vec{E}_j = 0 \quad (j=1,2), \tag{1}$$

$$E_j(z,t) = \tfrac{1}{2}\mathcal{E}_j(z,t)\exp[\omega_j t - k_j z + \phi_j(z,t)] + \text{c.c.}(j=1,2), \tag{2}$$

where ω_j are the angular frequencies of the laser fields and $\mathcal{E}_j(z,t)$ and $\phi_j(z,t)$ are slowly variable functions of z and t (see for example [10]).

The effect of the buffer gas is taken into account (i) by the relaxation rates γ_1 and γ_2 of the ground-states population difference and coherence, respectively [11] (ii) by the decay rate of the excited state (homogeneous broadening of $|m\rangle$), (iii) by the ''localization'' of atoms on the microwave wavelength scale (Dicke effect [12]).

The Zeeman sublevels in the ground state are resolved by the static magnetic field $\vec{B}_0$, while the hyperfine level $F'=1$ in the excited state is assumed uncoupled from the optical fields; Δ_0 is the laser detuning from the optical resonance.

The atomic ensemble prepared in the coherent superposition of the ground-state levels is coupled to a cylindrical microwave cavity to detect the coherent emission at the hyperfine frequency generated by the oscillating magnetization along $\hat{z}$ of the medium [6]. The cavity mode considered in the computations is the TE_{011}, whose magnetic field component $H_z(z)$ along the z axis is nearly constant inside the cell volume excited by the laser beams.

We analyze the atomic system in the ensemble-averaged density-matrix formalism [11] with the rotating wave approximation; the off-diagonal coherence terms are expressed as

$$\begin{aligned}
\rho_{\mu\mu'}(z,t) &= \delta_{\mu\mu'}(z,t)\exp\{i[(\omega_1-\omega_2)t \\
&\quad -(k_1-k_2)z + \phi_1(z,t) - \phi_2(z,t)]\}, \\
\rho_{\mu m}(z,t) &= \delta_{\mu m}(z,t)\exp\{i[\omega_1 t - k_1 z + \phi_1(z,t)]\}, \\
\rho_{\mu' m}(z,t) &= \delta_{\mu' m}(z,t)\exp\{i[\omega_2 t - k_2 z + \phi_2(z,t)]\},
\end{aligned} \tag{3}$$

where, as usual, $\delta_{\mu\mu'}$, $\delta_{\mu m}$, and $\delta_{\mu' m}$ are slowly varying functions of z and t. Inside an optically thick medium the amplitudes and the phases of the optical fields evolve according to the Maxwell equations that may be expressed in this case [10] as

$$\begin{aligned}
\frac{\partial\omega_{R1}}{\partial z} + \frac{1}{c}\frac{\partial\omega_{R1}}{\partial t} &= \alpha_1 \,\text{Im}\,\delta_{\mu m}, \\
\frac{\partial\phi_1}{\partial z} + \frac{1}{c}\frac{\partial\phi_1}{\partial t} &= -\frac{\alpha_1}{\omega_{R1}}\,\text{Re}\,\delta_{\mu m}, \\
\frac{\partial\omega_{R2}}{\partial z} + \frac{1}{c}\frac{\partial\omega_{R2}}{\partial t} &= \alpha_2 \,\text{Im}\,\delta_{\mu' m}, \\
\frac{\partial\phi_2}{\partial z} + \frac{1}{c}\frac{\partial\phi_2}{\partial t} &= -\frac{\alpha_2}{\omega_{R2}}\,\text{Re}\,\delta_{\mu' m},
\end{aligned} \tag{4}$$

having defined the optical Rabi angular frequencies,

$$\begin{aligned}
\omega_{R1} &= \mathcal{E}_1\langle\mu|e\hat{r}\cdot e_\lambda|m\rangle/\hbar, \\
\omega_{R2} &= \mathcal{E}_2\langle\mu'|e\hat{r}\cdot\hat{e}_\lambda|m\rangle/\hbar,
\end{aligned} \tag{5}$$

and the absorption parameters,

$$\alpha_1=\frac{\omega_1\langle\mu|e\hat{r}\cdot\hat{e}_\lambda|m\rangle^2}{\varepsilon_0\hbar c}n,$$

$$\alpha_2=\frac{\omega_2\langle\mu'|e\hat{r}\cdot\hat{e}_\lambda|m\rangle^2}{\varepsilon_0\hbar c}n, \tag{6}$$

where n is the atomic density of the medium, ε_0 the electric permettivity of vacuum, c the speed of light in vacuum, and $\hat{r}$ is the vector between the nucleus and the electron of the atom.

The evolution of the density matrix operator $\hat{\rho}$ is given by the Liouville equation that leads to a set of differential equations for the population and coherence terms; following the procedure reported in [6,7,8] and taking into account Eq. (3) we have

$$\rho_{\mu\mu}+\rho_{\mu'\mu'}\approx 1,\quad \Delta=\rho_{\mu'\mu'}-\rho_{\mu\mu},$$

$$\dot{\rho}_{mm}+\Gamma^*\rho_{mm}=-\omega_{R1}\,\mathrm{Im}\,\delta_{\mu m}-\omega_{R2}\,\mathrm{Im}\,\delta_{\mu' m},$$

$$\dot{\Delta}+\gamma_1\Delta=-2b\,\mathrm{Im}(e^{-i\Phi}\delta_{\mu\mu'})+\omega_{R2}\,\mathrm{Im}\,\delta_{\mu' m}-\omega_{R1}\,\mathrm{Im}\,\delta_{\mu m},$$

$$\dot{\delta}_{\mu\mu'}+[\gamma_2+i(\Omega_\mu+\dot{\phi}_1-\dot{\phi}_2)]\delta_{\mu\mu'}=i\frac{b}{2}e^{i\Phi}\Delta+i\frac{\omega_{R1}}{2}\delta_{m\mu'}-i\frac{\omega_{R2}}{2}\delta_{\mu m},$$

$$\dot{\delta}_{\mu m}+\left(\frac{1}{2}\Gamma^*+i\Delta_0\right)\delta_{\mu m}=-i\frac{\omega_{R1}}{4}(1-\Delta)-i\frac{\omega_{R2}}{2}\delta_{\mu\mu'},$$

$$\dot{\delta}_{\mu' m}+\left(\frac{1}{2}\Gamma^*+i\Delta_0\right)\delta_{\mu' m}=-i\frac{\omega_{R2}}{4}(1+\Delta)-i\frac{\omega_{R1}}{2}\delta_{\mu'\mu}. \tag{7}$$

The above set of equations has been derived in the hypothesis that $\omega_{Rj}(z,t)\ll\Gamma^*,\forall z,\ t(j=1,2)$, widely satisfied in the usual frequency standard applications. The "microwave detuning" $\Omega_\mu=(\omega_1-\omega_2)-\omega_{\mu'\mu}$ has been also assumed always negligible with respect to the excited state linewidth as well as the microwave Rabi frequency b defined as

$$b=\frac{1}{\hbar}\mu_0\mu_z H_z \tag{8}$$

and associated with the microwave magnetic field in the cavity,

$$\vec{B}=\hat{z}\mu_0 H_z\cos[(\omega_1-\omega_2)t+\Phi(t)], \tag{9}$$

where μ_0 is the permeability of free space and μ_z the hyperfine transition magnetic moment. In the case of alkali atoms for $m_F=0$, $\Delta m_F=0$ transition we have $\mu_z=\mu_B$, the Bohr magneton. We assume that $\omega_{\mu'\mu}$ is the hyperfine separation shifted by the static field $\vec{B}_0$, by the buffer gas collisions and any other time-independent perturbation. The field $\vec{B}$, in absence of external microwave fields applied to the atoms, is the microwave field generated by the atoms themselves; the phase term $\Phi(t)$ leads to the complex Rabi frequency,

$$\tilde{b}=be^{i\Phi} \tag{10}$$

and its full expression will be made explicit in the following analysis in the frame of a self-consistent approach of the CPT maser.

The set of Eq. (7) is very similar to the one examined in [7], but now all the density-matrix elements and the optical Rabi frequencies are functions of z and t.

In the case of an optically thin atomic sample and a cell length much shorter than the microwave wavelength ($L\ll\lambda$) the solution of the Maxwell equations for the microwave magnetic field in the cavity gives [7]

$$b=-2k|\delta_{\mu\mu'}|, \tag{11}$$

$$\Phi=\frac{\pi}{2}+\tan^{-1}\psi+\tan^{-1}\frac{\mathrm{Im}\,\delta_{\mu\mu'}}{\mathrm{Re}\,\delta_{\mu\mu'}}. \tag{12}$$

In Eq. (11) k is the number of microwave photons emitted by an atom in $1s$. Its expression is

$$k=\frac{\mu_0\mu_z^2\eta' Q_L n}{\hbar(2I+1)} \tag{13}$$

Q_L being the loaded cavity quality factor, η' the filling factor defined in [6], and I the nuclear spin. In Eq. (12) ψ is the detuning parameter of the cavity,

$$\psi=2Q_L\frac{\Delta\omega_c}{\omega_{\mu'\mu}}, \tag{14}$$

where $\Delta\omega_c$ is the cavity detuning from $\omega_{\mu'\mu}$; $\psi\ll 1$ in usual operating conditions ($\tan^{-1}\psi\cong\psi$).

Relations (11) and (12) may also be written in the more compact form

$$\tilde{b}=-2ike^{i\psi}\delta_{\mu\mu'}. \tag{15}$$

The total power generated by the atoms P_a in the cavity is then [6],

$$P_a=\frac{1}{2}\hbar\omega_{\mu'\mu}N_a\frac{|\tilde{b}|^2}{k}, \tag{16}$$

where N_a is the number of atoms in the effective volume of the cell exposed to the radiation fields.

For an optically thick atomic system, Eq. (15) is no longer valid but an equivalent expression may be found as follows.

We divide the cell containing the atomic sample in m elementary cells of length L/m with $m\gg 1$, as shown in Fig. 2.

For the TE_{011} mode the filling factor in the cell region ($L<d$) is proportional to the elementary cell length (L/m) and we can write for the jth cell $\eta'_j=\eta'/m$ and from Eq. (13) $k_j=k/m$.

Moreover, each elementary cell is optically thin so that Eq. (11) is valid,

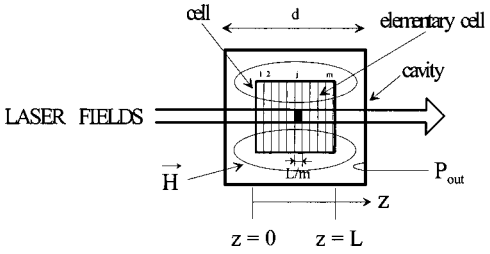

FIG. 2. Ideal elementary cells considered in the text.

$$b_j = -2k_j |\delta_{\mu\mu'}|_j \tag{17}$$

and Eq. (12) may be written as

$$\phi_j = \frac{\pi}{2} + \psi + \tan^{-1}\left(\frac{\mathrm{Im}\,\delta_{\mu\mu'}}{\mathrm{Re}\,\delta_{\mu\mu'}}\right) - (k_1 - k_2)z_j + [\phi_1(z,t) - \phi_2(z,t)]_j, \tag{18}$$

where the last two terms in the right-hand side take into account that the microwave phase is now referred at the laser fields phase difference that evolves along z as given by Eq. (2).

In compact form Eqs. (17) and (18) may be written as

$$\tilde{b}_j = -2ie^{i\psi}k_j(\delta_{\mu\mu'})_j e^{-2i\pi z_j/\lambda} \exp\{i[\phi_1(z,t) - \phi_2(z,t)]_j\}. \tag{19}$$

The total Rabi frequency associated with the standing microwave field excited in the cavity is given by the sum of the contributions from all the elementary cells and in the limit of $m \to \infty$ we have

$$\tilde{b}(t) = -2ie^{i\psi}\frac{k}{L}\int_0^L \delta_{\mu\mu'}(z,t)e^{-2i\pi z/\lambda} \times \exp\{i[\phi_1(z,t) - \phi_2(z,t)]\}\, dz. \tag{20}$$

We note that $\tilde{b}(t)$ does not depend on z as expected, being the microwave field supported by the cavity a standing wave.

The set of coupled Eqs. (4), (7), and (20) gives the general solution for the complete description of the CPT maser in a self-consistent approach in the case of an optically thick atomic medium. Through Eq. (16), the output power and the emission profile of the CPT maser may be evaluated both in steady state and in transient operation and all the main effects affecting its behavior may be examined (light shift, power broadening, microwave shift, cavity pulling, . . .) also in view of applications in time and frequency metrology. Using the adiabatic approximation, where the optical coherences are assumed to evolve much faster than the ground-state coherence, taking into account that $\alpha_1 \approx \alpha_2 = \alpha$ for the D_1 transition of alkali atoms and assuming $\Delta_0 = 0$ (lasers tuned to the optical transitions) the set of coupled equations turns out to be

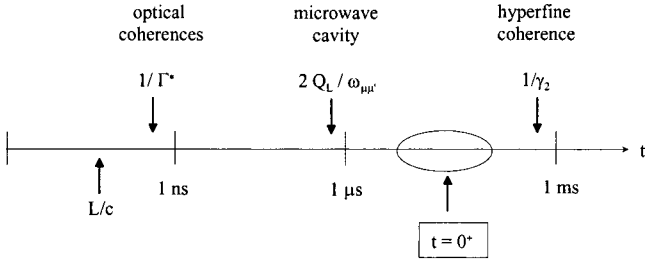

FIG. 3. Order of magnitude of the main time constants involved in the theory.

$$\frac{\partial\Delta}{\partial t} + \left(\gamma_1 + \frac{\omega_{R1}^2 + \omega_{R2}^2}{2\Gamma^*}\right)\Delta = -2\,\mathrm{Im}(\tilde{b}^*\delta_{\mu\mu'}) + \frac{\omega_{R1}^2 - \omega_{R2}^2}{2\Gamma^*},$$

$$\frac{\partial\delta_{\mu\mu'}}{\partial t} + \left[\gamma_2 + \frac{\omega_{R1}^2 + \omega_{R2}^2}{2\Gamma^*} + i\left(\Omega_\mu + \frac{\partial(\phi_1 - \phi_2)}{\partial t}\right)\right]\delta_{\mu\mu'} = i\frac{\tilde{b}}{2}\Delta - \frac{\omega_{R1}\omega_{R2}}{2\Gamma^*},$$

$$\frac{\partial\omega_{R1}}{\partial z} + \frac{1}{c}\frac{\partial\omega_{R1}}{\partial t} = -\frac{\alpha}{2\Gamma^*}[\omega_{R1}(1-\Delta) + 2\omega_{R2}\,\mathrm{Re}\,\delta_{\mu\mu'}],$$

$$\frac{\partial\omega_{R2}}{\partial z} + \frac{1}{c}\frac{\partial\omega_{R2}}{\partial t} = -\frac{\alpha}{2\Gamma^*}[\omega_{R2}(1+\Delta) + 2\omega_{R1}\,\mathrm{Re}\,\delta_{\mu\mu'}],$$

$$\frac{\partial(\phi_1 - \phi_2)}{\partial z} + \frac{1}{c}\frac{\partial(\phi_1 - \phi_2)}{\partial t} = -\frac{\alpha}{\Gamma^*}\left(\frac{\omega_{R2}}{\omega_{R1}} + \frac{\omega_{R1}}{\omega_{R2}}\right)\mathrm{Im}\,\delta_{\mu\mu'},$$

$$\tilde{b} = -2ie^{i\psi}\frac{k}{L}\int_0^L \delta_{\mu\mu'}e^{-2i\pi z/\lambda}e^{i(\phi_1 - \phi_2)}dz. \tag{21}$$

In order to solve the above system of coupled nonlinear differential equations it is necessary to fix the boundary conditions. We choose to fix the initial conditions at $z = 0^+ \forall t$ and at $t = 0^+ \forall z$, which allow us to reduce the problem to known physical limits. In fact at $z = 0^+$ the medium is optically thin $\forall t$ and the solutions are provided by the equations reported in [7]; in the case of equal laser intensities at the entrance of the cell we have,

$$\omega_{R1}(z = 0^+, t) = \omega_{R2}(z = 0^+, t) = \omega_R(0),$$

$$\phi_1(z = 0^+, t) - \phi_2(z = 0^+, t) = 0,$$

$$\dot{\Delta} + \left(\gamma_1 + \frac{\omega_R^2(0)}{\Gamma^*}\right)\Delta = -2\,\mathrm{Im}(\tilde{b}^*\delta_{\mu\mu'}),$$

$$\dot{\delta}_{\mu\mu'} + \left[\gamma_2 + \frac{\omega_R^2(0)}{\Gamma^*} + i\Omega_\mu\right]\delta_{\mu\mu'} = -\frac{\omega_R^2(0)}{2\Gamma^*} + \frac{i}{2}\tilde{b}\Delta\,. \tag{22}$$

The boundary conditions at $t = 0^+$ require to clear up the meaning of $t = 0^+$ from the physical point of view. In Fig. 3

we show the main time constants involved in the maser operation and the assumed physical origin of the time scale ($t=0^+$) for the analysis of the maser transient behavior.

We choose $t=0^+$ when the hyperfine coherence is not yet established while the optical coherences are at their steady-state condition and follow adiabatically the hyperfine one; the boundary conditions at $t=0^+$ are then provided by the classical solutions of an optically thick medium (Beer's law) in steady-state conditions,

$$\omega_{R1}(z,t=0^+)=\omega_{R2}(z,t=0^+)=\omega_R(0)e^{-(\alpha/2\Gamma^*)z},$$

$$\phi_1(z,t=0^+)-\phi_2(z,t=0^+)=0,$$

$$\Delta(z,t=0^+)=0,$$

$$\delta_{\mu\mu'}(z,t=0^+)=0. \tag{23}$$

In both Eqs. (22) and (23) thermodynamic equilibrium is assumed to be reached before the interaction with the laser fields.

III. NUMERICAL SOLUTIONS

A. Steady-state solutions

We consider in this section the output power, the line shape, and the frequency shift of the maser emission profile through the steady-state solution ($\partial/\partial t\rightarrow 0$) of the set of Eqs. (21).

1. Low-density case ($\alpha\rightarrow 0, L\approx\lambda$)

The case $\alpha\rightarrow 0$ and $L\ll\lambda$ (long-wavelength approximation) has been widely examined in [7] and in this case the Eqs. (21) reduce to the equations there reported. Here we analyze the effects related to the propagation of the laser beams inside a cell with $L\approx\lambda$. For a low-density medium and equal laser intensities at $z=0$ Eqs. (21) yield,

$$\omega_{R1}(z)=\omega_{R2}(z)=\omega_R(0) \quad \forall\ z,$$

$$\phi_1(z)-\phi_2(z)=0 \quad \forall\ z,$$

$$\tilde{b}=-2ik\delta_{\mu\mu'}\frac{\sin\pi L/\lambda}{\pi L/\lambda}e^{i(\psi-\pi L/\Lambda)},$$

$$(\gamma_1+2\Gamma_p)\Delta=-4k|\delta_{\mu\mu'}|^2\frac{\sin\pi L/\lambda}{\pi L/\lambda}\cos(\psi-\pi L/\lambda),$$

$$(\gamma_2+2\Gamma_p+i\Omega_\mu)\delta_{\mu\mu'}=-\Gamma_p+k\Delta\frac{\sin\pi L/\lambda}{\pi L/\lambda}\times e^{i(\psi-\pi L/\lambda)}\delta_{\mu\mu'}, \tag{24}$$

where $\Gamma_p=\omega_R^2(0)/2\Gamma^*$ is the transversal pumping rate.

The last two equations have a very interesting solution when $\psi-\pi L/\lambda=\pi/2$,

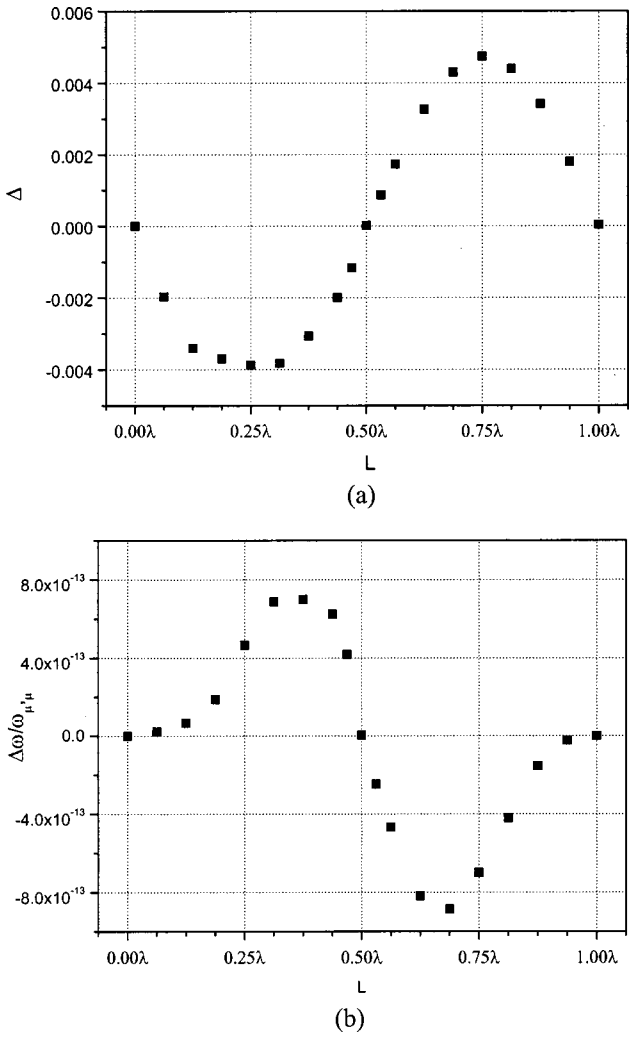

FIG. 4. (a) Computed population difference Δ and (b) propagation shift vs the cell length L, for the particular case: $\gamma_2=200\,\mathrm{s}^{-1}$, $\Gamma_p=200\,\mathrm{s}^{-1}$, and $k=10^3L\ \mathrm{s}^{-1}$.

$$\Delta(z)=0,$$

$$\delta_{\mu\mu'}(z)=\frac{-\Gamma_p}{\gamma_2+2\Gamma_p+i\Omega_\mu}. \tag{25}$$

It means that the proper choice of the cell length $L\approx\lambda/2$ eliminates the effects related to the feedback of the cavity on the atomic ensemble. In particular, this choice eliminates the unbalance in the ground-state populations that is responsible of the following effects on the maser emission profile $P_a(\Omega_\mu)$: the cavity pulling, when $\psi\neq 0$, and the microwave shift, when $\Delta_0\neq 0$. From Eq. (25), the shape of $P_a(\Omega_\mu)$ turns out Lorentzian. The more general solution of Eq. (24) gives the results shown in Fig. 4 for the population difference Δ and for the relative shift $\Delta\omega/\omega_{\mu'\mu}$ of the maser emission profile (propagation shift) vs the length of the atomic medium.

The solutions reported in Fig. 4 refer to the case of ^{87}Rb in buffer gas at low density; only for a cell of length $L \approx \lambda/2$ no unbalance in the populations is present and the maser emission profile is centered at the hyperfine transition frequency. The vertical axes for Δ and $\Delta\omega/\omega_{\mu'\mu}$ at a first approximation scale as k and k^2, as can be deduced from Eqs. (24). For the cell with $L \approx 0$ or $L \approx \lambda$ the third equation of Eq. (24) gives no output power; for $L=0$ it is obvious while for $L \approx \lambda$ the result may be understood in the following way: the elementary magnetizations emit with a position-dependent phase and sum up in such a way that the total magnetization is reduced to zero for a cell length $L \approx \lambda$. The general expression for the output power in this case is given by

$$P_a = \frac{1}{2}\hbar\omega_{\mu'\mu}N_a k|2\delta_{\mu\mu'}|^2\left(\frac{\sin \pi L/\lambda}{\pi L/\lambda}\right)^2. \qquad (26)$$

2. High-density case

In this case the system (21) has to be solved with the time derivatives equal zero and all the equations are coupled with each other. Due to the last integral equation, we have solved numerically the system with a recursive approach on the Rabi frequency $\tilde{b}$. We report in this subsection some numerical evaluations regarding the power generated by the atomic ensemble and the shifts of the emission profile center frequency.

The numerical values of the parameters used in the computations refer to the ^{87}Rb D_1 optical transition (electric dipole moment $d=1.5\times10^{-29}$ C/m) and to a buffer gas mixture (10 Torr of N_2 and 15 Torr of Ar for thermal compensation of the collision induced hyperfine frequency shift). In this case we may assume [11] $\Gamma^*=3\times10^9\,\mathrm{s}^{-1}$ and $\gamma_1 \approx \gamma_2 \approx 180\,\mathrm{s}^{-1}$ at $T=30\,^\circ$C; above this temperature γ_1 and γ_2 are controlled also by spin exchange and increase linearly with the atomic density n. We assume also a cell length $L \approx \lambda/2 \approx 2.2$ cm and a cavity loaded Q factor $Q_L = 15\,000$. With a laser beam radius of 1.3 cm the active volume is $N_a = 12\,\mathrm{cm}^3$ and the filling factor $\eta' \approx 0.2$. In order to fix the orders of magnitude, for the parameters considered above, we find at 60 °C; $n=3\times10^{11}\,\mathrm{cm}^{-3}$, $k=240\,\mathrm{s}^{-1}$, $\alpha=5.8\times10^{11}\,\mathrm{m}^{-1}\,\mathrm{s}^{-1}$, and $N_a=9\times10^{11}$.

The microwave power generated by the atomic ensemble vs the transversal pumping rate is reported in Fig. 5 for different atomic densities; equal laser intensities are assumed at the entrance of the cell. The saturation of the emitted power level vs Γ_p, typical of the CPT maser emission, is present also in this case of optically thick medium and the asymptotic level is proportional to n^2 as far as enough laser intensity is applied to the atomic system. The reported power levels are calculated at the peak of the emission profile.

The computed full width at half maximum $\Delta\nu_{1/2}$ of the emission profile is reported in Fig. 6 vs the atomic density; the significant reduction of the linewidth for increasing densities is an interesting consequence related to the EIT effect [3] which is embodied in the CPT phenomenon and has been observed experimentally in [8,13] for dark transitions in optically thick media. In Fig. 6 we report the ground state relaxation rate of the Rb atoms in the buffer gas [curve (a)] which makes evident the ''subnatural'' level achievable by the emission profile linewidth [curve (b)] when the atomic density is increased above a certain value in the case of a pure three-level system [14]. Besides the physical interest for this phenomenon always related to the EIT effect, the corresponding high atomic Q factor turns out of particular importance for the possible metrological applications of the CPT maser.

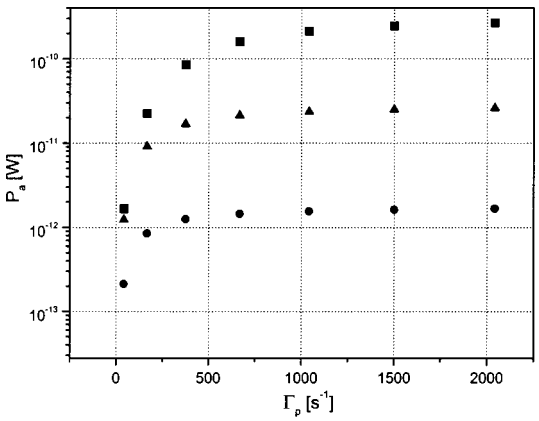

FIG. 5. Calculated emitted power vs the pumping rate for different atomic densities. ■, $n=3\times10^{11}\,\mathrm{cm}^{-3}$ ($T=60\,^\circ$C); ▲, $n=1.1\times10^{11}\,\mathrm{cm}^{-3}$ ($T=48\,^\circ$C); ●, $n=2.9\times10^{10}\,\mathrm{cm}^{-3}$ ($T=34\,^\circ$C).

The curve (c) of Fig. 6 refers to a real atomic system where the Zeeman degeneracy is assumed to be completely resolved; it has been evaluated in a phenomenological way from Eq. (21) via a reduction of the hyperfine coherence weight in the Maxwell equations by the factor $\xi=2I+1$ (I is the nuclear spin).

We report in Fig. 7 the behavior of the emission profile linewidth vs the optical Rabi frequency for two atomic density values in the subnatural regime. It turns out that in this case a power narrowing of the atomic transition has to be

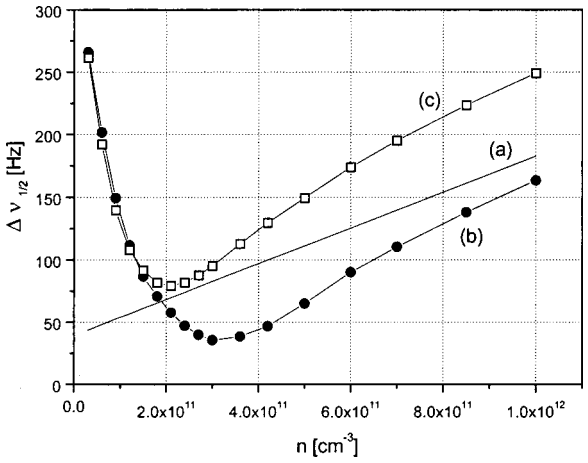

FIG. 6. Full width at half maximum of the CPT maser emission profile vs the atomic density. (a) natural linewidth of Rb atoms in buffer gas, γ_2/π; (b) linewidth in pure three-level system, ($\xi=1$); (c) same as (b) but taking into account the Zeeman structure of Rb atoms, as explained in the text ($\xi=1/4$); $\Gamma_p(0)=500\,\mathrm{s}^{-1}$.

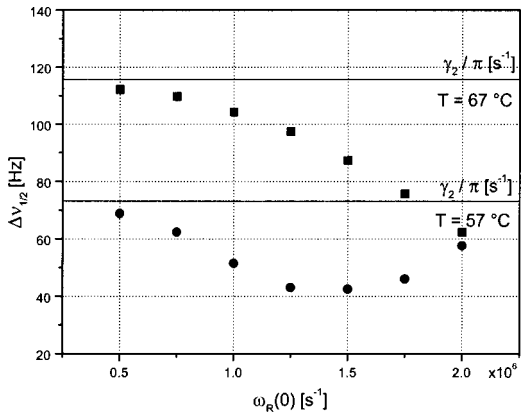

FIG. 7. Full width at half maximum of the maser emission profile vs the Rabi frequency. ■, $n=5.3\times10^{11}\,\mathrm{cm}^{-3}$; ●, $n=2.4\times10^{11}\,\mathrm{cm}^{-3}$.

observed which represents a signature of the subnatural regime itself.

When the atomic density is maintained fixed and k is varied through η' or Q_L [Eq. (13)] the solution of Eq. (21) leads to a broadening of the emission profile vs k, that is to the microwave broadening discussed in [7] for the case of an optically thin medium. In the present case this effect is slightly reduced and completely masked when k is varied through the atomic density n.

In Sec. III A 1 we have observed the existence of a propagation shift whose behavior vs the cell length is reported in Fig. 4(b). When the atomic ensemble is thick this shift becomes quite significant also for $L\approx\lambda/2$ as can be seen in Fig. 8.

This effect should be analyzed in greater detail in case of metrological applications and in particular its dependence from the various parameters which control the CPT maser behavior, in order to evaluate its influence on the final stability of the frequency standard.

We conclude the analysis of the steady-state solutions of the set of Eqs. (21) considering the effects on $P(\Omega_\mu)$ of the microwave cavity detuning ($\psi\neq0$ cavity pulling) and of the laser center frequency detuning ($\delta_0\equiv2\Delta_0/\Gamma^*\neq0$ microwave shift) always for equal laser intensities at the cell entrance. Typical results are for the cavity pulling $\Delta\omega/\omega_{\mu'\mu}\approx5\times10^{-11}$ with $\psi=0.1$ and for the microwave shift $\Delta\omega/\omega_{\mu'\mu}\approx5\times10^{-12}$ with $\delta_0=0.01$, when $n=1.1\times10^{11}\,\mathrm{cm}^{-3}$ [when $\delta_0\neq0$ the set of Eqs. (4), (7), and (20) has to be used].

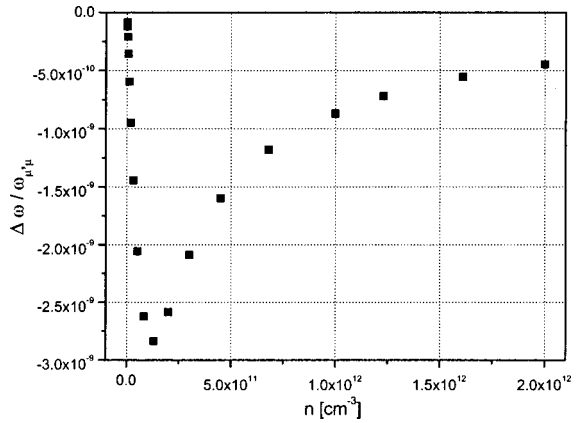

FIG. 8. Calculated propagation shift vs the atomic density for $\Gamma_p(0)=500\,\mathrm{s}^{-1}$.

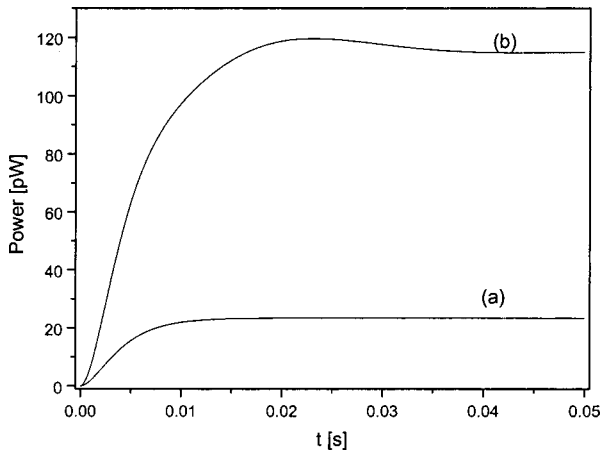

FIG. 9. Transient behavior of the power emitted by the CPT maser. $n=3\times10^{11}\,\mathrm{cm}^{-3}$, $L=0.03\,\mathrm{m}$, $\Gamma^*=3\times10^9\,\mathrm{s}^{-1}$, $\Gamma_p=200\,\mathrm{s}^{-1}$, (a) $\gamma_2=260\,\mathrm{s}^{-1}$, $k=300\,\mathrm{s}^{-1}$, (b) $\gamma_2=200\,\mathrm{s}^{-1}$, $k=1000\,\mathrm{s}^{-1}$.

We may conclude that the cavity pulling and the microwave shift as well as the power broadening of the emission profile reduce their contribution in an optically thick medium with respect to an optically thin one [7] and that they are negligible when compared with the propagation shift. This last effect is due to the dependence of the phases of the elementary magnetization from the position inside the active volume and is described by the term $\exp[i(2\pi z/\lambda)]\exp[i(\phi_1-\phi_2)]$ of Eq. (20). In principle, this effect could be eliminated or at least strongly reduced by use of a coated cell without buffer gas [11] where a motional averaging for the elementary magnetization phases may be assumed (random motion of the atoms through the laser wave fronts).

B. Dynamical solutions

The calculated output power buildup of the CPT maser reported in Fig. 9 is obtained from the numerical solution of the system (21) with boundary conditions (22) and (23). When the reduced gain parameter k/γ_2 and the pumping rate Γ_p/γ_2 reach values of the order of 1 an overshoot is present in the output transient response as shown in Fig. 9(b); this feature was already present in the case of an optically thin medium [7], but now its duration is extended in time by the effect of the atomic density.

It is interesting to note that a similar behavior has been reported for dark lines observed in optically thick media [15] and in that case it was a clear signature of the EIT effect; in particular, it may be also related to the very high group delay τ_g typical of these media as it has been theoretically predicted in [16] and experimentally observed in [17]. We may evaluate the group delay for the CPT maser starting from the Eqs. (21) and applying a sinusoidal amplitude perturbation of

the laser fields at the entrance of the cell. In particular, we express the first boundary condition of Eq. (22) as

$$\omega_{R1}(z=0^+)=\omega_{R2}(z=0^+)=\omega_R(z=0^+)[1+m_a\sin\omega_m t],$$

$$m_a \ll 1,$$

and we compute the delay between the output and the input perturbation signals. The calculated group delay vs the Fourier frequency $\omega_m/2\pi$ has a behavior analogous to the experimental curve reported later on (see Fig. 19). In particular, for a negligible cavity feedback and for $n=2.6\times10^{11}\,\mathrm{cm}^{-3}$, $L=5$ cm; $\omega_R(z=0^+)=1\times10^6\,\mathrm{s}^{-1}$, and $m_a=0.1$, we calculated a time group delay of about 2 ms, corresponding to a group velocity of the order of 20 m/s. The group delay bandwidth is of the order of the maser emission linewidth and any information contained in such a bandwidth is delayed in time with negligible distortion. In the case of Fig. 9 the observed overshoot may well be related to the delayed (and distorted) transmission of the amplitude step applied to the laser fields for the analysis of the transient behavior.

IV. COMPARISON BETWEEN CPT AND IOP MASERS

In this section we extend the calculations also to the case of the IOP maser, which may be easily derived from the theory reported in Sec. II. A deeper understanding of the CPT stimulated emission phenomenon is obtained from the comparison with the IOP maser as it was already observed in the case of an optically thin medium [7].

The IOP maser equations may be deduced from Eq. (21) taking into account that:

(a) $\omega_{R2}(z=0^+)=0\ \forall\ t$;

(b) the phases of the elementary magnetizations are forced by the microwave field that builds up in the cavity and not by the laser fields phase difference.

With reference to point (a), in principle, a field at ω_2 may be generated inside an optically thick medium (Raman gain) but, in absence of an optical resonant cavity, the feedback of the field at ω_2 on the atomic ensemble is fully negligible so that we assume

$$\omega_{R2}(z,t)=0\quad\forall\quad z,t. \tag{27}$$

As far as point (b) is concerned, the complex microwave Rabi frequency in this case turns out to be

$$\tilde{b}(t)=-2ike^{i\psi}\frac{1}{L}\int_0^L\delta_{\mu\mu'}(z,t)dz. \tag{28}$$

Inserting Eqs. (27) and (28) in Eq. (21), we obtain the set of differential equations that describe the IOP maser behavior in a complete self-consistent approach for the case of an optically thick atomic ensemble. In steady-state conditions $(\partial/\partial t\to0)$ we have

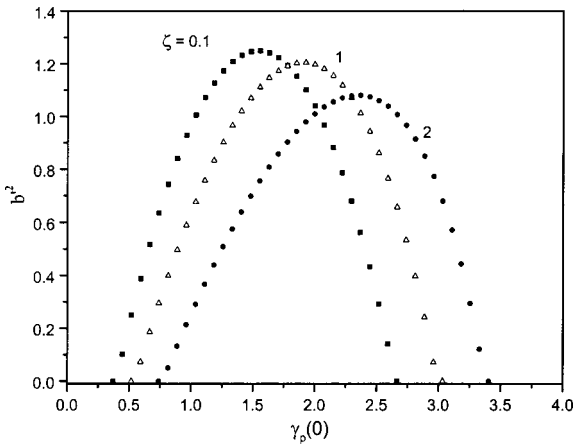

FIG. 10. Numerical solutions of Eq. (30) vs $\gamma_p(0)$, with $k'=5$.

$$\left(\gamma_1+\frac{\omega_{R1}^2}{2\Gamma^*(1+\delta_0^2)}\right)\Delta=-2\,\mathrm{Im}(\tilde{b}^*\delta_{\mu\mu'})+\frac{\omega_{R1}^2}{2\Gamma^*},$$

$$\left[\gamma_2+\frac{\omega_{R1}^2}{2\Gamma^*(1+\delta_0^2)}+i\left(\Omega_\mu+\frac{\omega_{R1}^2}{2\Gamma^*}\frac{\delta_0}{1+\delta_0^2}\right)\right]\delta_{\mu\mu'}=i\frac{\tilde{b}}{2}\Delta,$$

$$\frac{\partial\omega_{R1}}{\partial z}=-\frac{\alpha\omega_{R1}}{2\Gamma^*}\frac{1-\Delta}{1+\delta_0^2},$$

$$\tilde{b}=-2ie^{i\psi}\frac{k}{L}\int_0^L\delta_{\mu\mu'}dz. \tag{29}$$

In the above equations $\omega_{R1}^2(z)/2\Gamma^*=\Gamma_p(z)$ is now the longitudinal pumping rate; in the particular case $\delta_0=0$ and $\psi=0$, assuming $\gamma_1\approx\gamma_2$ and $\Omega_\mu=0$ (natural maser emission frequency), the following analytical solution of Eq. (29) is found (see Appendix):

$$\ln\left\{e^{-\zeta/k'}-\frac{1-e^{-\zeta/k'}}{\gamma_p(0)}(b'^2+1)\right\}-(1-e^{-\zeta/k'})$$
$$\times[1+b'^2+\gamma_p(0)]+\frac{\zeta}{k'}b'^2+\zeta=0, \tag{30}$$

where $\zeta=\alpha L/\Gamma^*$ is the optical length of the medium; $k'=k/\gamma_2$ is the (reduced) gain factor; $\gamma_p(0)=\Gamma_p(0)/\gamma_2$ is the initial (reduced) longitudinal pumping rate; and $b'=|\tilde{b}|/\gamma_2$ is the (reduced) complex Rabi frequency, which gives the power generated by the atoms through Eq. (16).

Numerical solutions of Eq. (30) are reported in Fig. 10 that represents the behavior of the generated power vs the pumping rate; for an optically thin medium ($\zeta=0.1$) we find the parabolic curve already reported in [7] while for an optically thick medium ($\zeta>1$) the optimum output power is shifted towards higher pumping rates. Moreover, the emission threshold and the corresponding pumping rate are reported in Fig. 11 vs the optical length as obtained always from Eq. (30).

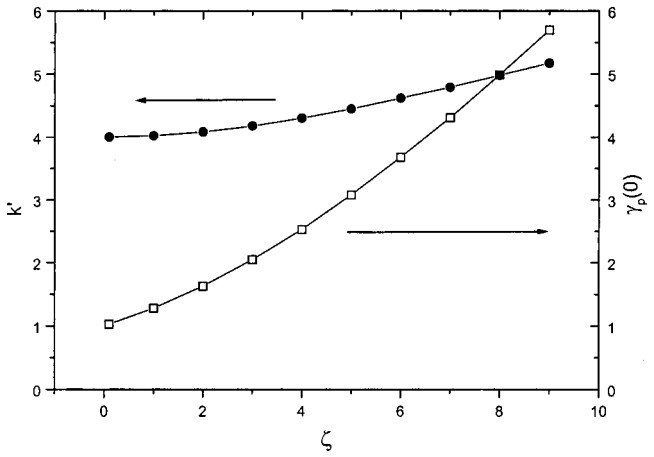

FIG. 11. Emission threshold and corresponding pumping rate vs the optical length ζ. □, $\gamma_p(0)=\Gamma_p(0)/\gamma_2$; ●, $k'=k/\gamma_2$.

We observe that the main effect of the optical length on the IOP maser is a slight increase of the threshold condition and a higher pumping rate required to achieve the maximum output power. No propagation shift arises in this case and this is the new difference between CPT and IOP masers when the optical length is not negligible; this difference from the physical point of view reflects the different constraints for the phases of the elementary magnetizations. In fact in the IOP maser they are defined by the internally generated microwave field while in the CPT maser they are fixed to the local phase difference of the optical fields.

V. EXPERIMENTAL RESULTS

A. Experimental apparatus

The experiments have been done with the setup shown in Fig. 12.

A semiconductor diode laser with an external Littman-Metcalf cavity provides a tunable radiation at 795 nm (D_1 ^{87}Rb transition) and a power of up to 10 mW that is coupled through an isolator to an electro-optic modulator (EOM) via a single mode polarization maintaining optical fiber.

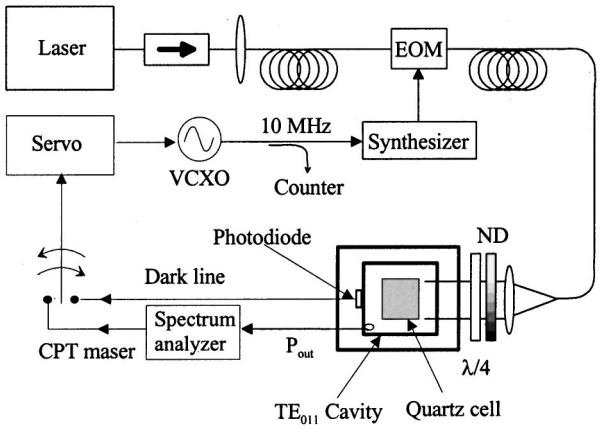

FIG. 12. The experimental setup: EOM, electro-optic modulator; VCXO, voltage controlled crystal oscillator; ND, neutral density attenuators.

The EOM has a rf bandwidth of 5 GHz and allows to reach a phase modulation index of $m_\phi \approx 4$ with 1 W of rf power; applying to the EOM the output of a microwave synthesizer at 3.417 GHz ($\nu_{\mu'\mu}/2$) the first two modulation sidebands of the output spectrum provide the radiation fields at ω_1 and ω_2 required for the Λ excitation scheme when the laser is tuned to the D_1 center of gravity. The two radiations are phase coherent between themselves as required by Eq. (2) and have equal intensities so that $\omega_{R1}(z=0^+)=\omega_{R2}(z=0^+)$ when the excited optical level is the $5\ ^2P_{1/2}F'=2$; with a modulation index $m_\phi \approx 2.4$ the laser carrier is suppressed. The power of the modulated laser spectrum at the entrance of the cavity is 700 μW and the beam shape is a TEM_{00} Gaussian mode with a e^{-1} radius of 10 mm. A λ/4 plate provides the $\sigma^{\pm}$ polarization required to excite the $\Delta m_F=0$ microwave transitions [18].

The quartz cell has an internal length of $L=18$ mm and contains ^{87}Rb (98%) and a thermally compensated buffer gas mixture (15.5 Torr of Ar and 9.5 Torr of N_2).

The microwave cavity is made of Al and is tuned to $\omega_{\mu'\mu}/2\pi$ for the TE_{011} mode; when the quartz cell is inserted and the coupling is critical the loaded quality factor turns out $Q_L=10\,000$ at the operating temperature of 60 °C. The cell is provided of a cold finger that avoids a significant coating of the inside surface by the rubidium atoms. From the data above reported the cavity filling factor turns out $\eta' \approx 0.4$ and the active volume $V_a=5.6\ \mathrm{cm}^3$; in the low density limit $\gamma_2/\pi \approx 70$ Hz.

The cavity is temperature controlled and placed inside a double magnetic shield; a longitudinal static magnetic field $B_0 \approx 10^{-5}$ T defines the quantization axis.

The transmitted optical fields, detected by a photodiode, provide an absorption signal useful to lock the laser frequencies to the optical transitions ($\Delta_0=0$, not indicated in Fig. 12), and/or the dark line signal which may be used to lock the microwave synthesizer on the hyperfine ^{87}Rb transition. The CPT microwave emission is detected by a spectrum analyzer that may act as a heterodyne detector to analyze the transient behavior of the CPT maser or to lock the microwave synthesizer to the atomic emission profile.

B. Experimental results

The spectrum of the microwave emission shown in Fig. 13 has been observed at $T=77$ °C ($n \approx 10^{12}\ /\mathrm{cm}^3, \gamma_2/\pi = 230$ Hz, $k \approx 1000\ \mathrm{s}^{-1}$) and with $\Gamma_p \approx 700\ \mathrm{s}^{-1}$; it is centered at $(\omega_1-\omega_2)/2\pi$ and its width is limited by the resolution bandwidth of the spectrum analyzer. The signal to noise ratio for an observation bandwidth of 1 Hz is 25 000 and is limited by the thermal noise of the cavity and of the detection system.

Taking into account the cavity coupling and the external losses, the power generated by the atoms is $P_a \approx 20$ pW, not far from the theoretical estimations for the present experimental configuration.

The maser output power vs the transversal pumping rate is shown in Fig. 14 for three different atomic densities; the

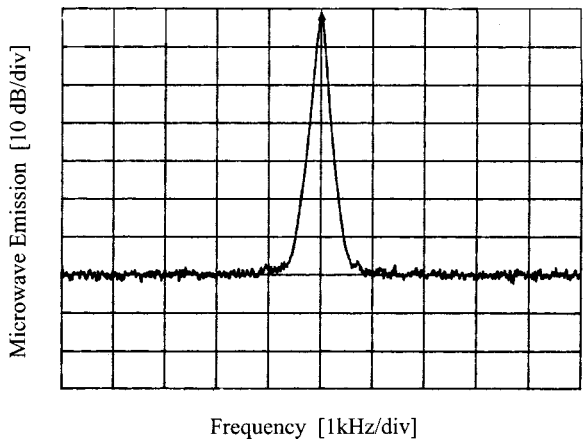

FIG. 13. Spectrum of the microwave emission. Power at the peak, 6.3 pW; vertical axis, 10 dB/div; horizontal axis, 1 kHz div; center frequency, 6.834 687 GHz; resolution bandwidth, 100 Hz; video bandwidth, 100 Hz.

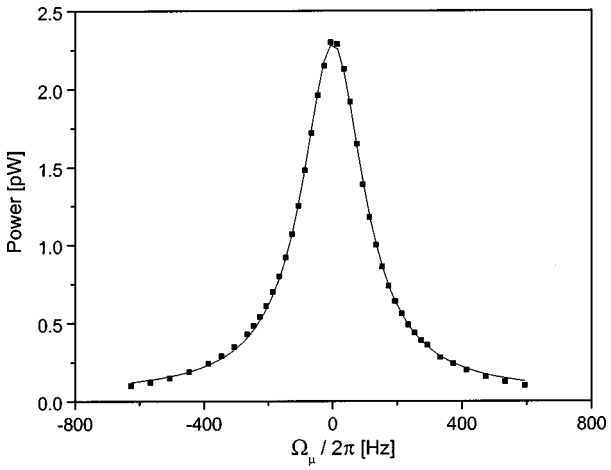

FIG. 15. Maser emission profile. ■, experimental points; ——, Lorentzian fit; $\Gamma_p = 500\,\mathrm{s}^{-1}$.

behavior is in agreement with the computations reported in Fig. 5 while, as far as the absolute values of the vertical axis are concerned, the remarks reported for Fig. 13 are still valid.

The power emission profile vs the microwave detuning $\Omega_\mu/2\pi$ is an important feature of the CPT maser because it is centered to the ground-state frequency splitting; the experimental curve shown in Fig. 15 refers to a cell temperature $T = 68\,^\circ\mathrm{C}$ ($n \approx 6\times10^{11}\ \mathrm{cm}^{-3}, \gamma_2/\pi = 150$ Hz).

The experimental points are fitted with a Lorentzian curve; the full width at half maximum is $\Delta\nu_{1/2} \approx 240$ Hz. The slight asymmetry observed in the experimental profile may be due both to a position dependent residual light-shift or to the non linearities of the thick medium and increases with the pumping rate. The observed linewidth is reduced with respect to the low density value $(\gamma_2 + 2\Gamma_p)/\pi \approx 470$ Hz [6] as predicted by the theoretical computations and already reported in the experiments with the dark line [19]. A subnatural linewidth has been also observed for a limited range of pumping rates as reported in Fig. 16. At low pumping rates it is clearly observed the power narrowing of the atomic transition predicted in the numerical computations of Fig. 7.

It is worth noticing that the applied laser beams can easily determinate some optical pumping between the hyperfine sublevels, leaving a degree of uncertainty in the real population of the $m_F = 0$ ground-state levels.

A more detailed physical and experimental description of this phenomenon is reported in [19]. The significant linewidth reduction for any pumping rate value observed in the high-density regime is relevant for the high resolution spectroscopy and especially for the atomic frequency standard field, where the opportunity of working with high-Q resonances is particularly desirable.

Another typical feature of the CPT maser emission is the propagation shift; as reported in Sec. III of this paper, when the long-wavelength approximation does not hold for the atomic sample ($L \sim \lambda$) the peak of the emission profile is shifted with respect to $\omega_{\mu'\mu}/2\pi$ due to the dependence of the elementary magnetization phases from the position inside the active volume. This effect is not present obviously in the

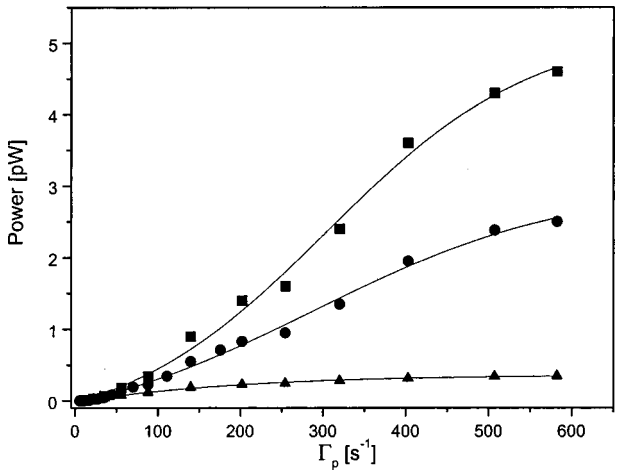

FIG. 14. Maser output power. ■, $T = 77\,^\circ\mathrm{C}$ ($n = 1.1\times10^{12}\,\mathrm{cm}^{-3}$); ●, $T = 68\,^\circ\mathrm{C}$ ($n = 6\times10^{11}\,\mathrm{cm}^{-3}$); ▲, $T = 47\,^\circ\mathrm{C}$ ($n = 8\times10^{10}\,\mathrm{cm}^{-3}$).

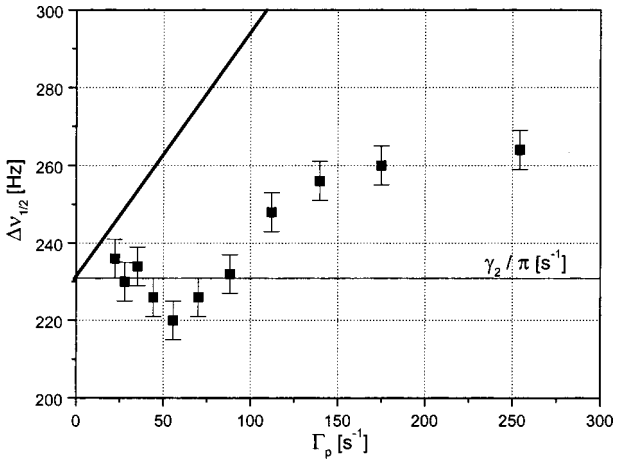

FIG. 16. Maser emission profile linewidth. ■, experimental points at $T = 77\,^\circ\mathrm{C}$ ($n = 1.1\times10^{12}\,\mathrm{cm}^{-3}$); ——, natural linewidth; ——, low-density theory.

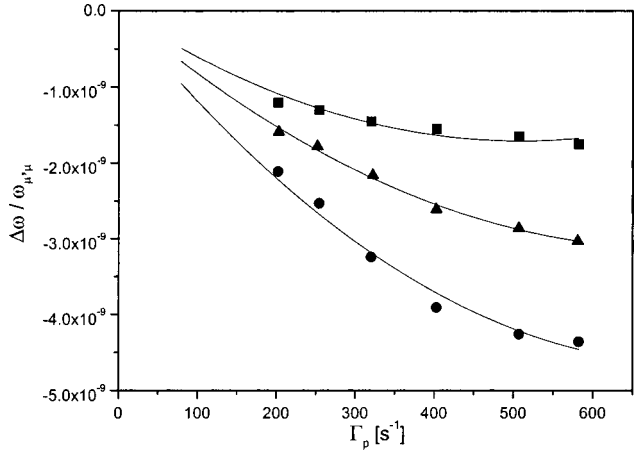

FIG. 17. Measured propagation shift. ■, $T=47\,^{\circ}\mathrm{C}$ ($n=8\times10^{10}\,\mathrm{cm}^{-3}$); ▲, $T=68\,^{\circ}\mathrm{C}$ ($n=6\times10^{11}\,\mathrm{cm}^{-3}$); ●, $T=77\,^{\circ}\mathrm{C}$ ($n=1.1\times10^{12}\,\mathrm{cm}^{-3}$).

dark line signal so that we have been able to observe it locking the synthesizer alternatively to the maser emission profile and to the dark line.

The experimental measurements reported in Fig. 17 show the observed behavior of the propagation shift vs the pumping rate at different atomic densities. The magnitude of the shift is in the range of the theoretical values reported in Fig. 8 and increases with the atomic density; this behavior, predicted by the theory only for lower densities ($n<2\times10^{11}\,\mathrm{cm}^{-3}$), could be due to the fact that the real system is not a pure three-level system as assumed in the theory. It is worth while mentioning that we have been able to compensate the above red shift in our apparatus with the blue light shift induced by the off resonant components of the modulated laser spectrum [20]; this compensation is highly desirable in view of applications in the frequency standard field.

The transient behavior of the output microwave power is shown in Fig. 18 for a $\Gamma_p\approx500\,\mathrm{s}^{-1}$, $T=68\,^{\circ}\mathrm{C}$ ($n=6\times10^{11}\,\mathrm{cm}^{-3}$) and shows the typical overshoot predicted in the theory (see Fig. 9) and discussed in the previous section.

We report finally in Fig. 19 the measured group delay for

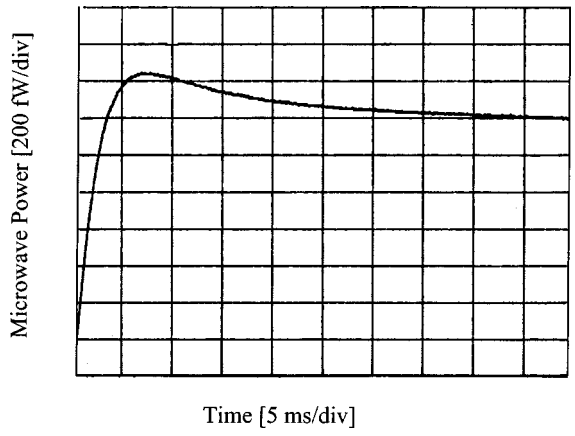

FIG. 18. Output power as measured in transient mode. Vertical axis, 200 fW/div; horizontal axis, 5 ms/div. Resolution bandwith, 10 kHz; video bandwidth, 10 kHz.

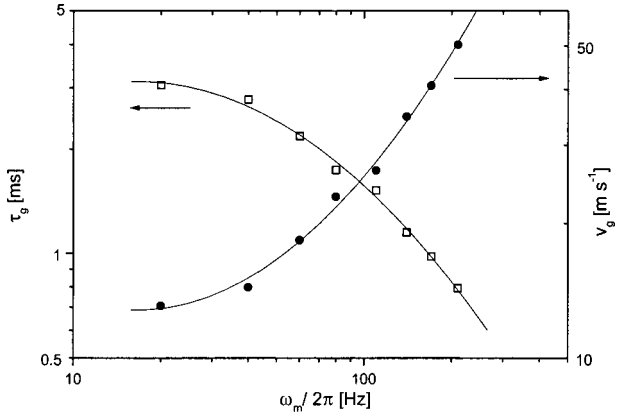

FIG. 19. Group delay and velocity versus the Fourier frequency of the amplitude perturbation. $T=67\,^{\circ}\mathrm{C}$ ($n=5.3\times10^{11}\,\mathrm{cm}^{-3}$), $\Gamma_p\approx200\,\mathrm{s}^{-1}$, $\Omega_\mu=0$.

a sinusoidal amplitude perturbation applied at the laser fields; it turns out in good agreement with the theoretical computations.

We have used in the case of Fig. 19 a cell with a length $L=4$ cm to increase the sensitivity of the experiment: the emission profile width is $\Delta\nu_{1/2}\approx100$ Hz and the output power is strongly reduced by the propagation term $(\sin\pi L/\lambda)/(\pi L/\lambda)$ [see for example Eq. (26)] at the level of 1 fW. The measured group delay anyway is of the order of $\tau_g=(\pi\Delta\nu_{1/2})^{-1}$ as may be easily computed for the case of an optically thin atomic medium in the long-wavelength approximation and without cavity feedback.

The group delay measured at a fixed Fourier frequency vs the microwave detuning $\Omega_\mu/2\pi$ is reported in Fig. 20 and shows an apparent superluminal propagation ($\tau_g<0$) when $\Omega_\mu/2\pi\approx-\Delta\nu_{1/2}$.

Negative group delays are indeed present in the numerical solutions of Eq. (21) for the parameter's range used in the experiments. Here we do not go further in the examination of this phenomenon widely considered in the recent literature [21], but we only remark that the CPT maser emission may be a useful tool to pursue these studies, being a direct observation of the ground-state coherence; moreover the high sen-

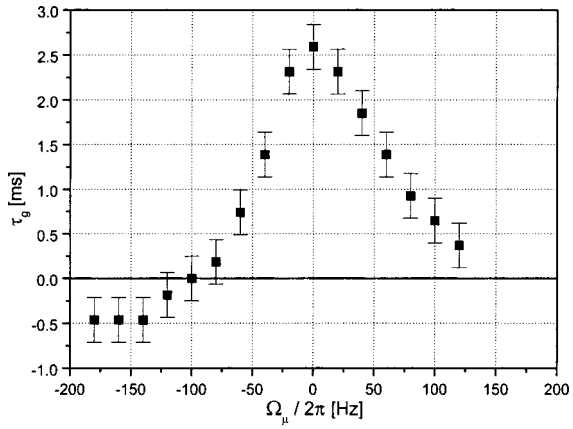

FIG. 20. Group delay versus the microwave detuning. $T=67\,^{\circ}\mathrm{C}$ ($n=5.3\times10^{11}\,\mathrm{cm}^{-3}$), $\Gamma_p\approx200\,\mathrm{s}^{-1}$, $\omega_m/2\pi=30$ Hz.

sitivity of the heterodyne detection technique and the absence of any laser background allow looser constraints for the experimental apparatus.

VI. CONCLUSIONS

In this paper we have developed a fully self-consistent theory of the CPT maser in the case of an optically thick active medium and a cell length comparable with the microwave wavelength. The atomic density limits the effects of the cavity feedback, examined in [7] in the case of an optically thin medium, and, in particular, the microwave broadening of the emission profile, the cavity pulling and the microwave shift are significantly reduced.

We have found that the laser fields propagation inside a cell of length $L \approx \lambda$ leads in general to a shift of the emission profile with respect to the hyperfine transition frequency (propagation shift); in the low-density case this shift may be controlled through a proper choice of the cell length while in the higher density case a coated cell or a suitably modulated laser spectrum are probably the only solution to reduce this shift that otherwise represents a serious drawback for the realization of a frequency standard with high-medium-term stability.

A strong benefit for the atomic Q factor comes from the significant narrowing predicted for the emission profile when the atomic density increases due to the EIT effect, up to reach a subnatural linewidth. The theory reported in this paper may be used as a starting point for a practical realization of an atomic frequency standard with a medium-term stability significantly better than that of an IOP maser or of a classical frequency standard based on rf-optical double resonance.

The numerical results refer to ^{87}Rb atoms in buffer gas but the theory here reported applies not only to other alkali-metal atoms but to any three-level closed system which satisfies the assumptions made in Sec. II. The experimental results have been found in good agreement with the theoretical predictions and in particular the observation of the subnatural linewidth and of the propagation shift. Finally we have also reported the observation of an apparent superluminal propagation in presence of a suitable microwave detuning.

ACKNOWLEDGMENTS

The authors wish to thank J. Vanier for helpful and stimulating discussions and N. Beverini and E. Maccioni for the help in filling the rubidium cells. This work was partially supported by ASI (Italian Space Agency).

APPENDIX

In the particular case considered in Sec. IV, the system (29) may be written as

$$\Delta = \frac{\Gamma_p(\gamma_2+\Gamma_p)}{(\gamma_2+\Gamma_p)^2+|\tilde{b}|^2}, \tag{A1}$$

$$\delta_{\mu\mu'} = i\frac{\tilde{b}}{2}\frac{\Gamma_p}{(\gamma_2+\Gamma_p)^2+|\tilde{b}|^2}, \tag{A2}$$

$$\frac{\partial\Gamma_p}{\partial z} = -\frac{\alpha\Gamma_p(1-\Delta)}{\Gamma^*}, \tag{A3}$$

$$\tilde{b} = -2i\frac{k}{L}\int_0^L \delta_{\mu\mu'}dz, \tag{A4}$$

where Δ, Γ_p, and $\delta_{\mu\mu'}$ are functions of z.

Inserting (A1) and (A3) we obtain,

$$\frac{\partial\Gamma_p}{\partial z} = -\frac{\alpha\Gamma_p}{\Gamma^*}\frac{\gamma_2(\gamma_2+\Gamma_p)+|\tilde{b}|^2}{(\gamma_2+\Gamma_p)^2+|\tilde{b}|^2}, \tag{A5}$$

while inserting (A2) in (A4) we have

$$\tilde{b} = -2i\frac{k}{L}\int_0^L i\frac{\tilde{b}}{2}\frac{\Gamma_p}{(\gamma_2+\Gamma_p)^2+|\tilde{b}|^2}dz.$$

The microwave Rabi frequency does not depend on z, so that the above equation, neglecting the solution $\tilde{b}=0$, becomes,

$$\frac{k}{L}\int_0^L \frac{\Gamma_p}{(\gamma_2+\Gamma_p)^2+|\tilde{b}|^2}dz = 1. \tag{A6}$$

The differential equation (A5) with the boundary condition $\Gamma_p(z=0)=\Gamma_p(0)$ has the following solution:

$$\log\frac{\Gamma_p(L)}{\Gamma_p(0)} + \frac{\Gamma_p(0)}{\gamma_2}\left[\frac{\Gamma_p(L)}{\Gamma_p(0)}-1\right] - \frac{|\tilde{b}|^2}{\gamma_2^2}\log\frac{\gamma_2[\gamma_2+\Gamma_p(L)]+|\tilde{b}|^2}{\gamma_2[\gamma_2+\Gamma_p(0)]+|\tilde{b}|^2} = -\frac{\alpha L}{\Gamma^*}. \tag{A7}$$

The differential equation (A5) may also be written in the form,

$$-\frac{\Gamma^*}{\alpha}\frac{d\Gamma_p}{\gamma_2(\gamma_2+\Gamma_p)+|\tilde{b}|^2} = \frac{\Gamma_p dz}{(\gamma_2+\Gamma_p)^2+|\tilde{b}|^2},$$

which may be introduced in (A6) and, after integration over the cell length, we obtain

$$\log\frac{\gamma_2[\gamma_2+\Gamma_p(L)]+|\tilde{b}|^2}{\gamma_2[\gamma_2+\Gamma_p(0)]+|\tilde{b}|^2} = -\frac{\alpha L}{\Gamma^*}\frac{\gamma_2}{k}. \tag{A8}$$

First of all at this point we may introduce (A8) in (A7) obtaining the simplified relation,

$$\log\frac{\Gamma_p(L)}{\Gamma_p(0)}+\frac{\Gamma_p(0)}{\gamma_2}\left[\frac{\Gamma_p(L)}{\Gamma_p(0)}-1\right]+\frac{\alpha L}{\Gamma^*}\left(1+\frac{\gamma_2}{k}\frac{|\tilde{b}|^2}{\gamma_2^2}\right)=0, \tag{A9}$$

then we solve (A8) for $\Gamma_p(L)$ and introduce its expression in (A9).

Using finally the reduced definitions $\gamma_p(0)$, k' and b' and the optical length ζ, we obtain Eq. (30) which gives the IOP maser output $|\tilde{b}|^2$ in a fully self-consistent approach in the case of an optically thick medium.

[1] G. Alzetta, A. Gozzini, L. Moi, and G. Orriols, Nuovo Cimento Soc. Ital. Fis., B **36**, 5 (1976).

[2] M. O. Scully, Phys. Rep. **219**, 191 (1992).

[3] K.-J. Boller, A. Imamolu, and S. E. Harris, Phys. Rev. Lett. **66**, 2593 (1991).

[4] A. Godone, F. Levi, and J. Vanier, Phys. Rev. A **59**, R12 (1999).

[5] A. Godone, F. Levi, and J. Vanier, IEEE Trans. Ultrason. Ferroelectr. Freq. Control **46**, 609 (1999).

[6] J. Vanier, A. Godone, and F. Levi, Phys. Rev. A **58**, 2345 (1998).

[7] A. Godone, F. Levi, S. Micalizio, and J. Vanier, Phys. Rev. A **62**, 053402 (2000).

[8] A. Godone, F. Levi, S. Micalizio and J. Vanier (unpublished); A. Godone, F. Levi, S. Micalizio, and J. Vanier, in *Proceedings of the International Conference on Lasers 2000*, edited by V. J. Corcoran and T. A. Corcoran (STS Press, McLean, 2001), pp. 872–880.

[9] J. C. Camparo, J. Opt. Soc. Am. B **15**, 1177 (1998).

[10] M. O. Scully and M. S. Zubairy, *Quantum Optics* (Cambridge University Press, Cambridge, England, 1999).

[11] J. Vanier and C. Audoin, *The Quantum Physics of Atomic Frequency Standards* (Adam Hilger, Bristol, England, 1989).

[12] R. H. Dicke, Phys. Rev. **89**, 472 (1953).

[13] M. D. Lukin, Phys. Rev. Lett. **79**, 2959 (1997).

[14] C. L. Bentley, Jr., J. Liu, and Y. Liao, Phys. Rev. A **61**, 023811 (2000).

[15] H. X. Chen, Phys. Rev. A **58**, 1545 (1998).

[16] O. Kocharovskaya, Y. Rostovtsev, and M. O. Scully, Phys. Rev. Lett. **86**, 628 (2001).

[17] M. M. Kash, *et al.*, Phys. Rev. Lett. **82**, 5229 (1999).

[18] F. Levi, A. Godone, S. Micalizio, and G. Modugno, Eur. Phys. J. D **12**, 53 (2000).

[19] M. D. Lukin, M. Fleischauer, A. S. Zibrov, H. G. Robinson, V. L. Velichansky, L. Hollberg, and M. O. Scully, Phys. Rev. Lett. **79**, 2959 (1997); A. Godone, F. Levi, and S. Micalizio (unpublished).

[20] F. Levi, A. Godone, and J. Vanier, IEEE Trans. Ultrason. Ferroelectr. Freq. Control **47**, 466 (2000).

[21] A. Kuzmich, A. Dogariu, L. J. Wang, P. W. Milonni, and R. Y. Chiao, Phys. Rev. Lett. **86**, 3925 (2001); A. Dogariu, A. Kuzmich, and L. J. Wang, Phys. Rev. A **63**, 053806 (2001); D. Bortman-Arbiv, A. D. Wilson-Gordon, and H. Friedmann, *ibid.* **63**, 043818 (2001); M. Artoni, G. C. La Rocca, F. S. Cataliotti, and F. Bassani, *ibid.* **63**, 023805 (2001).